NEW DIFFRACTION ANOMALIES AND BACKSCATTERING RESONANCE ON A GRATING OF TRIANGULAR CROSS SECTION

S. Sesnic

and

S. Jovićević[+)]

IPP III/9 May 1973

MAX-PLANCK-INSTITUT FÜR PLASMAPHYSIK

GARCHING BEI MÜNCHEN

MAX-PLANCK-INSTITUT FÜR PLASMAPHYSIK

GARCHING BEI MÜNCHEN

NEW DIFFRACTION ANOMALIES AND BACKSCATTERING RESONANCE ON A GRATING OF TRIANGULAR CROSS SECTION

S. Sesnic

and

S. Jovićević[+)]

IPP III/9 May 1973

+) Tehnički Fakultet, Titograd, Yugoslavia

Die nachstehende Arbeit wurde im Rahmen des Vertrages zwischen dem Max-Planck-Institut für Plasmaphysik und der Europäischen Atomgemeinschaft über die Zusammenarbeit auf dem Gebiete der Plasmaphysik durchgeführt.

IPP III/9

S. Sesnic
S. Jovicevic

New Diffraction Anomalies and Backscattering Resonance on a Grating of Triangular Cross Section

(in English)

May 1973

Abstract

The solution to the problem of diffraction of a parallel- and perpendicular-polarized wave from an echelette grating is discussed with a special emphasis on diffraction anomalies. Two new kinds of anomalies are described. The first kind occuring when the phase change of the incident wave over the groove is equal to a multiple of π , the second kind occuring when this phase change is equal to an odd multiple of $\pi/2$. The first kind can coincide with a double Rayleigh anomaly, which then for a perpendicular-polarized wave results in an amplified anomaly. If additionaly one of the grating orders in the double Rayleigh anomaly is + 1 order, a resonant type anomaly results. This resonance anomaly could be utilized in laser cavity or for the purpose of the spectral or spatial filtering.

Table of Contents: Page

List of Figures :

Introduction

Ever since Wood[1] in 1902 published experimental results pointing to the anomalous behaviour of diffraction gratings, these anomalies were frequent object for theoretical and experimental studies. The reason for the interest in Wood anomalies was that the spectroscopist had to know them well in order not to misinterpret the spectrum he is obtaining in his experiment. Wood also found that these anomalies are evident only for the perpendicular polarization. In 1907, Lord Rayleigh[2] developed a diffraction theory and predicted theoretically the position of these anomalies, however, only for the perpendicular polarization. After him quite a few other authors worked on the theoretical explanation of the Wood anomalies. In more recent times many papers were published treating this subject. Palmer[3] was the first to thoroughly document the existence of the parallel anomalies. Yakovlev and Gerasimov[4] published a wealth of data on grating spectra and polarization effects of echolette gratings. Stewart and Gallaway studied the Wood anomalies[5]. Two different assumptions about the cause for the anomalies were utilized to explain these anomalies. In one case the anomalies were explained in terms of wave phenomena on infinite periodic structures. This approach was e.g. taken by Deriugin[6,7] in his discussion of the grating of a rectangular profile, where he assumed solution above the grating in terms of Fourier orders and in the groove region in terms of waveguide modes. The same method was utilized later for the same rectangular grating by Wirgin and Deleuil[8], whose work showed excellent agreement between the theory and experiment. Deleuil[9] also reported some measurements of grating spectra from a grating of a triangular profile and some anomalies from a rectangular grating. Utilizing guided wave approach Hessel and Oliner[10]

discovered the existence of two types of anomalies: already known Rayleigh anomaly and a new type of resonance anomaly related to guided complex waves supported by the grating. Other authors on the other hand proposed that the anomalies are a local phenomenon. Palmer, Evering and Nelson[11] in an early article believed that the anomalies are caused by a surface wave phenomene supported by the periodic structure of the grating, although, already at that point they had measurements of anomalies on gratings with only twelve lines. Twersky[12] has shown, using multiple scattering approach, that already two or more isolated grating elements may lead to anomalies. In 1968 Phelps and Palmer[13] showed experimentally that the anomalies are local phenomenon. On the basis of that fact they developed a simple theory for a rectangular grating[14], that shows a good agreement with the experiment. In the most recent work Palmer and LeBrun[15] show that the multiple scattering within the single grating groove can account for anomalous behaviour.

In this paper we use an earlier[16] developed method of solving diffraction grating problem rigorously for the purpose of studying the Rayleigh and new anomalies. In Sec.I we summarize the diffraction grating theory and develop new expressions for the coupling coefficients. Convergence of these coefficients is discussed. In Sec. II A new anomalies are discussed. It is shown, that they occur, when the phase difference of the incident wave across the groove is either an even or an odd multiple of $\pi/2$. In Sec. II B the coincidence of this new anomaly with the Rayleigh anomaly is investigated. In Sec. II C the numerical examples are presented.

I. Diffraction Theory for a Two-Dimensional Echelette Grating

Let us consider a monochromatic plane wave, incident on an infinite echelette grating made out of a perfect conductor. The wave is propagating in +x and -y directions. The angle of incidence is φ . The other grating parameters are as shown in Fig. 1. All the dimensions in the figure are normalized to the groove width d.

A general plane wave incident upon the grating can be decomposed into two linear polarizations: parallel polarization or P wave, that has the electric field parallel with the grooves, and perpendicular polarization or S wave, that is normal on the grooves. Each of these polarizations is discussed separately.

A. Parallel Polarization

The incident electric field has only z component and can be represented, dropping the subscript z, as

$$E_i(x,y) = E \exp[ik(\gamma x + \delta y) - i\omega t]. \qquad (1)$$

E is the amplitude of the incident wave, $k = 2\pi/\lambda$ is the wave number and γ and δ are direction sine and cosine defined by $\gamma = \sin\varphi$ and $\delta = -\cos\varphi$.

Because the grating is periodic in x with period $2\pi/d$ the diffracted wave can be represented in terms of space harmonics

$$E_r(x,y) = \sum_{n=-\infty}^{\infty} E_{rn} \exp[ik(\gamma_n x + \delta_n y) - i\omega t], \qquad (2)$$

where E_{rn} is the unknown amplitude of the nth harmonic, and

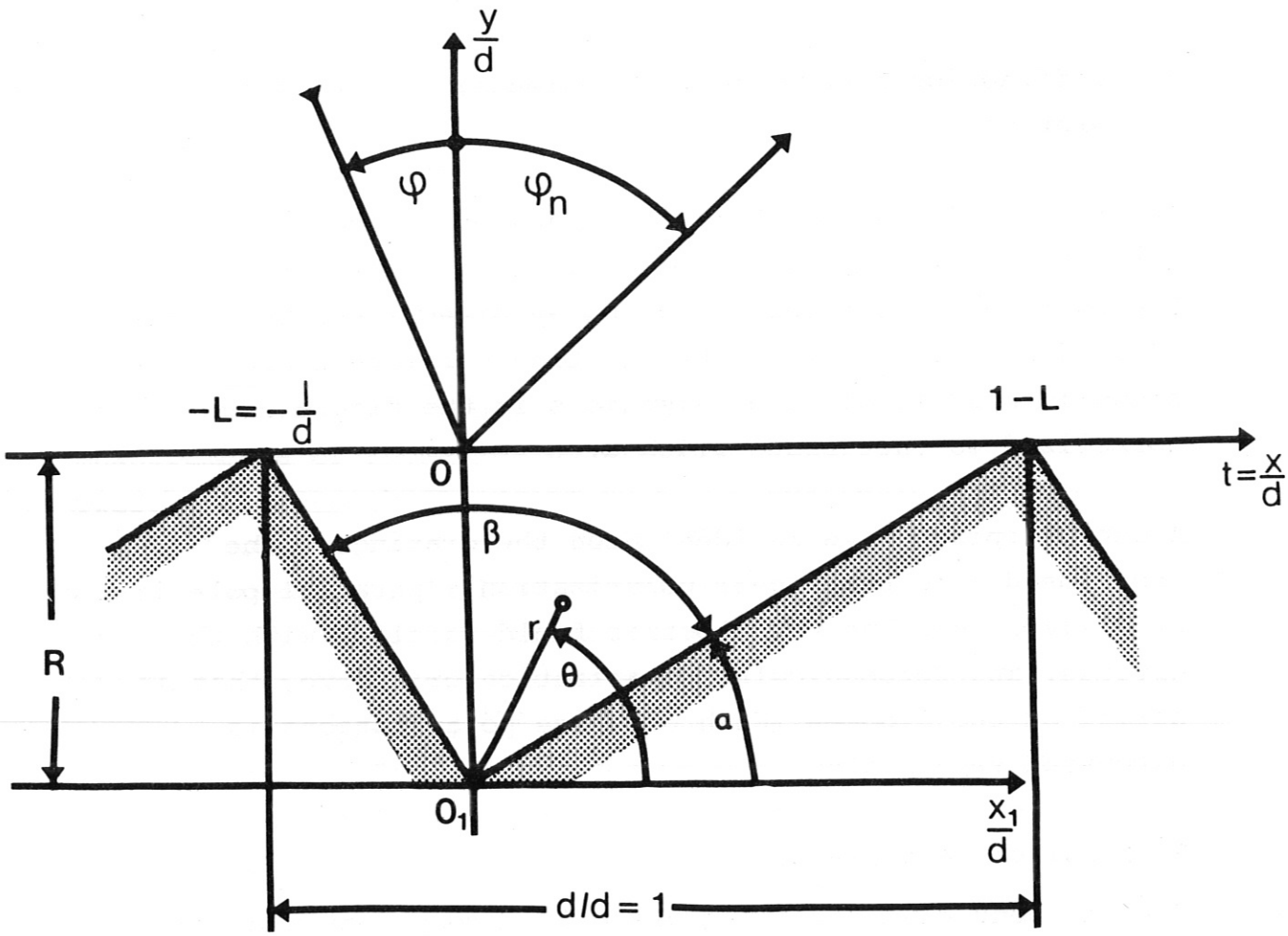

Fig. 1 Echelette grating groove geometry.

γ_n and δ_n are defined by

$$\gamma_n = \gamma - n\frac{\lambda}{d} \tag{3}$$

$$\delta_n = +(1 - \gamma_n^2)^{\frac{1}{2}}. \tag{4}$$

For n such that $|\gamma_n| \leq 1$ or δ_n positive real the expression (2) describes propagating outgoing waves. For larger n γ_n becomes larger than 1 and δ_n becomes positive imaginary. $|\gamma_n| > 1$ describes evanescent waves attenuated in +y direction.

Standing waves in the grooves can be represented in terms of wedge-modes, each satisfying the boundary conditions on the surface of the walls,

$$E_g(r,\theta) = \sum_{\ell=1}^{\infty} E_{g\ell} J_\nu(kr) \sin[\nu(\theta-\alpha)] \exp(-i\omega t), \tag{5}$$

where $E_{g\ell}$ is the unknown amplitude of the ℓth groove harmonic, $J_\nu(kr)$ is the Bessel function of the first kind, and $\nu = \ell\pi/\beta$, with ℓ = 1, 2, 3 .....

The corresponding incident, diffracted and groove magnetic fields can be found from Maxwell's equations utilizing (1), (2) and (5).

The unknown amplitudes E_{rn} and $E_{g\ell}$ can be found from the boundary conditions on the surface of the grating in the y = 0 plane. These boundary conditions request that both the electric- and magnetic-field components parallel to that plane be continuous across that plane.

The reflected harmonics E_{rn} are orthogonal so they can be isolated by multiplying the boundary condition for the electric field by $\exp[ik(\gamma_m x)]$ and integrating it in x from $-\ell$ to $d-\ell$.

Unfortunately, the groove harmonics $E_{g\ell}$ are not orthogonal, therefore, they cannot be isolated. Nevertheless, we multiply the boundary condition for the magnetic field by $J_\mu(kr)$ where $\mu = m\pi/\beta$ with m = 0, 1, 2 .... and integrate again in x from $-\ell$ to $d-\ell$. After doing some algebra this will result in an infinite set of linear equations for unknown groove harmonic amplitude $E_{g\ell}$ and in a set of equations for E_{rn}

$$\sum_{\ell=1}^{\infty} E_{g\ell}\left\{\sum_{n=-r}^{\infty} \delta_n b^{\rho}_{\ell n} a_{nm} - c^{\rho}_{\ell m}\right\} = -2E\delta a_{om} \qquad (6)$$

and

$$E_{rn} = \sum_{\ell=1}^{\infty} E_{g\ell} b^{\rho}_{\ell n} - \Delta_{on} E\,, \qquad (7)$$

where Δ_{on} is a Kronecker symbol, being equal to 1 for n = 0, otherwise zero. a_{nm}, $b^{\rho}_{\ell n}$ and $c^{\rho}_{\ell m}$ are matrix coefficients given by

$$a_{nm} = \int_{-L}^{1-L} \exp(iA\pi\gamma_n t)\, J_\mu[A\pi(t^2+R^2)^{\frac{1}{2}}]\, dt \qquad (8)$$

$$b^{\rho}_{\ell n} = \int_{-L}^{1-L} \exp(-iA\pi\gamma_n t)\, J_\nu[A\pi(t^2+R^2)^{\frac{1}{2}}] \sin\left[\nu\left(\tan^{-1}\frac{R}{t} - \alpha\right)\right] dt \qquad (9)$$

$$c^{\rho}_{\ell m} = -\frac{i}{2}\int_{-L}^{1-L} J_\mu[A\pi(t^2+R^2)^{\frac{1}{2}}]\left\{J_{\nu-1}[A\pi(t^2+R^2)^{\frac{1}{2}}]\cos\left[(\nu-1)\tan^{-1}\frac{R}{t} - \nu\alpha\right] + J_{\nu+1}[A\pi(t^2+R^2)^{\frac{1}{2}}]\cos\left[(\nu+1)\tan^{-1}\frac{R}{t} - \nu\alpha\right]\right\} dt\,. \qquad (10)$$

Coefficient A, describing inverse relative wavelength, is defined by $A = 2\,d/\lambda$.

In matrix and vector notation we define

$$\sum_{n=-\infty}^{\infty} \delta_n b^p_{\ell n} a_{nm} - c^p_{\ell m} = B^p_{\ell m} \longrightarrow [B]$$

$$b^p_{\ell n} \longrightarrow [b^p]$$

$$-2E\delta a_{om} \longrightarrow \vec{A}$$

so that (6) and (7) can be written

$$[B]\cdot\vec{E}_g = \vec{A}$$

$$\vec{E}_r = [b^p]\cdot\vec{E}_g - \vec{o}\,E$$

where $\vec{o}$ is the unit vector for n = 0.
Premultiplying (13a) by $[B]^{-1}$ we get

$$\vec{E}_g = [B]^{-1}\cdot\vec{A} .$$

Inserting into (13b) we obtain the diffracted fields:

$$\vec{E}_r = [b^p]\cdot[B]^{-1}\cdot\vec{A} - \vec{o}\,E .$$

The coefficients a_{nm}, $b^p_{\ell n}$ and $c^p_{\ell m}$, and the amplitude $E_{g\ell}$ and E_{rn} converge rather fast with n, m and ℓ so that the matrix equations (6) and (7) can be truncated. The equation (6) can be inverted and $E_{g\ell}$ found. Inserting $E_{g\ell}$ into (7) E_{rn} can also be found. Finally, one can evaluate the reflection coefficients for the nth order from

$$R^p_n = |E_{rn}|^2 \frac{\delta_n}{-\delta} . \qquad (11)$$

It is of interest to investigate the matrix elements on their convergence and also on their influence on anomalies. For this purpose it is of advantage to perform in expressions for a_{nm} and $b^{p}_{\ell n}$ integration by parts. One then obtains

$$
\begin{aligned}
a_{nm} = \Bigg\{ & \sin A\pi\gamma \sum_{k=0}^{\infty} \frac{(-1)^k}{(A\pi\gamma_n)^{2k+1}} \frac{d^{2k}}{dt^{2k}} J_\mu\left[A\pi(t^2+R^2)^{\frac{1}{2}}\right]\Big|_{t=1-L}^{+} \\
& + \cos A\pi\gamma \sum_{k=0}^{\infty} \frac{(-1)^k}{(A\pi\gamma_n)^{2k+2}} \frac{d^{2k+1}}{dt^{2k+1}} J_\mu\left[A\pi(t^2+R^2)^{\frac{1}{2}}\right]\Big|_{t=1-L}^{-} \\
& - \sum_{k=0}^{\infty} \frac{(-1)^k}{(A\pi\gamma_n)^{2k+2}} \frac{d^{2k+1}}{dt^{2k+1}} J_\mu\left[A\pi(t^2+R^2)^{\frac{1}{2}}\right]\Big|_{t=-L} \Bigg\} + \\
+ i \Bigg\{ & \sin A\pi\gamma \sum_{k=0}^{\infty} \frac{(-1)^k}{(A\pi\gamma_n)^{2k+2}} \frac{d^{2k+1}}{dt^{2k+1}} J_\mu\left[A\pi(t^2+R^2)^{\frac{1}{2}}\right]\Big|_{t=1-L}^{-} \\
& - \cos A\pi\gamma \sum_{k=0}^{\infty} \frac{(-1)^k}{(A\pi\gamma_n)^{2k+1}} \frac{d^{2k}}{dt^{2k}} J_\mu\left[A\pi(t^2+R^2)\right]\Big|_{t=1-L}^{+} \\
& + \sum_{k=1}^{\infty} \frac{(-1)^k}{(A\pi\gamma_n)^{2k+1}} \frac{d^{2k}}{dt^{2k}} J_\mu\left[A\pi(t^2+R^2)^{\frac{1}{2}}\right]\Big|_{t=-L} \Bigg\}
\end{aligned}
\tag{12}
$$

and

$$
\begin{aligned}
b^{p}_{\ell n} = \Bigg\{ & -\sin A\pi\gamma \sum_{k=0}^{\infty} \frac{(-1)^k}{(A\pi\gamma_n)^{2k+1}} \frac{d^{2k}}{dt^{2k}} \left[J_\nu\left[A\pi(t^2+R^2)^{\frac{1}{2}}\right] \sin\left[\nu\left(\tan^{-1}\frac{R}{t} - \alpha\right)\right] \right]\Big|_{t=1-L} \\
& + \cos A\pi\gamma \sum_{k=0}^{\infty} \frac{(-1)^k}{(A\pi\gamma_n)^{2k+2}} \frac{d^{2k+1}}{dt^{2k+1}} \left[J_\nu\left[A\pi(t^2+R^2)^{\frac{1}{2}}\right] \sin\left[\nu\left(\tan^{-1}\frac{R}{t} - \alpha\right)\right] \right]\Big|_{t=1-L} \\
& - \sum_{k=0}^{\infty} \frac{(-1)^k}{(A\pi\gamma_n)^{2k+2}} \frac{d^{2k+1}}{dt^{2k+1}} \left[J_\nu\left[A\pi(t^2+R^2)^{\frac{1}{2}}\right] \sin\left[\nu\left(\tan^{-1}\frac{R}{t} - \alpha\right)\right] \right]\Big|_{t=-L} \Bigg\} + \\
+ i \Bigg\{ & -\sin A\pi\gamma \sum_{k=0}^{\infty} \frac{(-1)^k}{(A\pi\gamma_n)^{2k+2}} \frac{d^{2k+1}}{dt^{2k+1}} \left[J_\nu\left[A\pi(t^2+R^2)^{\frac{1}{2}}\right] \sin\left[\nu\left(\tan^{-1}\frac{R}{t} - \alpha\right)\right] \right]\Big|_{t=1-L}^{-} \\
& - \cos A\pi\gamma \sum_{k=0}^{\infty} \frac{(-1)^k}{(A\pi\gamma_n)^{2k+1}} \frac{d^{2k}}{dt^{2k}} \left[J_\nu\left[A\pi(t^2+R^2)^{\frac{1}{2}}\right] \sin\left[\nu\left(\tan^{-1}\frac{R}{t} - \alpha\right)\right] \right]\Big|_{t=1-L}^{+} \\
& + \sum_{k=0}^{\infty} \frac{(-1)^k}{(A\pi\gamma_n)^{2k+1}} \frac{d^{2k}}{dt^{2k}} \left[J_\nu\left[A\pi(t^2+R^2)^{\frac{1}{2}}\right] \sin\left[\nu\left(\tan^{-1}\frac{R}{t} - \alpha\right)\right] \right]\Big|_{t=-L} \Bigg\} .
\end{aligned}
\tag{13}
$$

B. Perpendicular polarization

In the case of the perpendicular polarization the magnetic field will have its only component in z - direction. Therefore, in a similar fashion as for the parallel polarization, the incident, reflected, and the groove magnetic fields can be represented by

$$H_i(x,y) = H \exp[ik(\gamma x + \delta y) - i\omega t], \qquad (14)$$

$$H_r(x,y) = \sum_{n=-\infty}^{\infty} H_{rn} \exp[ik(\gamma_n x + \delta_n y) - i\omega t], \qquad (15)$$

and

$$H_g(r,\theta) = \sum_{\ell=0}^{\infty} H_{g\ell} J_\nu(kr) \cos[\nu(\theta - \alpha)] \exp(-i\omega t). \qquad (16)$$

By satisfying the boundary conditions at the surface of the grating and performing similar multiplications and integrations, the boundary conditions finally result in

$$\sum_{\ell=0}^{\infty} H_{g\ell} \left\{ \sum_{n=-\infty}^{\infty} \delta_n b^s_{\ell n} a_{nm} - c^s_{\ell m} \right\} = -2H\delta a_{om} \qquad (17)$$

and

$$H_{rn} = \sum_{\ell=0}^{\infty} H_{g\ell} b^s_{\ell n} - \Delta_{on} H. \qquad (18)$$

The expression for a_{nm} is the same as for the parallel case but the matrix coefficients $b^s_{\ell n}$ and $c^s_{\ell m}$ have a somewhat different form

$$b^s_{\ell n} = \int_{-L}^{1-L} \exp(-iA\pi\gamma_n t)\, J_\nu[A\pi(t^2+R^2)^{\frac{1}{2}}] \cos[\nu(\tan^{-1}\frac{R}{t} - \alpha)]\, dt \tag{19}$$

$$c^s_{\ell m} = \frac{i}{2}\int_{-L}^{1-L} J_\mu[A\pi(t^2+R^2)^{\frac{1}{2}}]\Big\{ J_{\nu-1}[A\pi(t^2+R^2)^{\frac{1}{2}}] \sin[(\nu-1)\tan^{-1}\frac{R}{t} - \nu\alpha] + \tag{20}$$
$$+ J_{\nu+1}[A\pi(t^2+R^2)^{\frac{1}{2}}] \sin[(\nu+1)\tan^{-1}\frac{R}{t} - \nu\alpha]\Big\}.$$

The relation (17) can be truncated in ℓ, m and n and inverted to obtain $H_{g\ell}$ and (18) can be truncated to obtain H_{rn}. Finally, one obtains again the reflection coefficient of the nth order

$$R^s_n = |H_{rn}|^2 \frac{\delta_n}{-\delta}\,. \tag{21}$$

The expression (19) can be again integrated by parts

$$\begin{aligned} b^s_{\ell n} = \Big\{ &-\sin A\pi\gamma \sum_{k=0}^{\infty} \frac{(-1)^k}{(A\pi\gamma_n)^{2k+1}} \frac{d^{2k}}{dt^{2k}} \Big[J_\nu[A\pi(t^2+R^2)^{\frac{1}{2}}]\cos[\nu(\tan^{-1}\tfrac{R}{t} - \alpha)]\Big]\Big|_{t=1-L}^{+} \\ &+ \cos A\pi\gamma \sum_{k=0}^{\infty} \frac{(-1)^k}{(A\pi\gamma_n)^{2k+2}} \frac{d^{2k+1}}{dt^{2k+1}} \Big[J_\nu[A\pi(t^2+R^2)^{\frac{1}{2}}]\cos[\nu(\tan^{-1}\tfrac{R}{t} - \alpha)]\Big]\Big|_{t=1-L}^{-} \\ &- \sum_{k=0}^{\infty} \frac{(-1)^k}{(A\pi\gamma_n)^{2k+2}} \frac{d^{2k+1}}{dt^{2k+1}} \Big[J_\nu[A\pi(t^2+R^2)^{\frac{1}{2}}]\cos[\nu(\tan^{-1}\tfrac{R}{t} - \alpha)]\Big]\Big|_{t=-L} \Big\} + \\ &+ i\Big\{ -\sin A\pi\gamma \sum_{k=0}^{\infty} \frac{(-1)^k}{(A\pi\gamma_n)^{2k+2}} \frac{d^{2k+1}}{dt^{2k+1}} \Big[J_\nu[A\pi(t^2+R^2)^{\frac{1}{2}}]\cos[\nu(\tan^{-1}\tfrac{R}{t} - \alpha)]\Big]\Big|_{t=1-L}^{-} \\ &- \cos A\pi\gamma \sum_{k=0}^{\infty} \frac{(-1)^k}{(A\pi\gamma_n)^{2k+1}} \frac{d^{2k}}{dt^{2k}} \Big[J_\nu[A\pi(t^2+R^2)^{\frac{1}{2}}]\cos[\nu(\tan^{-1}\tfrac{R}{t} - \alpha)]\Big]\Big|_{t=-L}^{} \Big\}. \end{aligned} \tag{22}$$

Expressions (12), (13) and (22) allow us now to discuss the convergence of these matrix coefficients. Note first that because $\gamma_n \sim n$ for large n the various terms in infinite sum will be proportional either to $\frac{1}{n^{2\ell+1}}$ or to $\frac{1}{n^{2\ell+2}}$.

Obviously for large n the strongest influence will be exerted by the lowest term in the infinite sum, i.e. by the term with $\ell = 0$. Remembering that

$$\sin\left[\nu\left(\tan^{-1}\frac{R}{t}-\alpha\right)\right]\Big|_{t=1-L} = \sin\left[\nu\left(\tan^{-1}\frac{R}{t}-\alpha\right)\right]\Big|_{t=-L} = 0$$

we can write in the lowest approximation by retaining only the $\ell = 0$ term:

$$a_{nmr} \sim \frac{1}{A\pi\gamma_n}\sin(A\pi\gamma)\,J_\mu\left[A\pi\sqrt{(1-L)^2+R^2}\right] \tag{23}$$

$$a_{nmi} \sim -\frac{1}{A\pi\gamma_n}\left[\cos(A\pi\gamma)\,J_\mu\left[A\pi\sqrt{(1-L)^2+R^2}\right) + J_\mu\left[A\pi\sqrt{L^2+R^2}\right]\right] \tag{24}$$

$$b^p_{enr} \sim \frac{1}{(A\pi\gamma_n)^2}\cos(A\pi\gamma)\frac{d}{dt}\left\{J_\nu\left(A\pi\sqrt{t^2+R^2}\right)\sin\left[\nu\left(\tan^{-1}\frac{R}{t}-\alpha\right)\right]\right\}\Big|_{t=1-L} - \frac{1}{(A\pi\gamma_n)^2}\frac{d}{dt}\left\{J_\nu\left(A\pi\sqrt{t^2+R^2}\right)\sin\left[\nu\left(\tan^{-1}\frac{R}{t}-\alpha\right)\right]\right\}\Big|_{t=-L} \tag{25}$$

$$b^p_{eni} \sim -\frac{1}{(A\pi\gamma_n)^2}\sin(A\pi\gamma)\frac{d}{dt}\left\{J_\nu\left[A\pi\sqrt{t^2+R^2}\right]\sin\left[\nu\left(\tan^{-1}\frac{R}{t}-\alpha\right)\right]\right\}\Big|_{t=1-L} \tag{26}$$

$$b^s_{enr} \sim \frac{1}{A\pi\gamma_n}\sin(A\pi\gamma)\,J_\nu\left(A\pi\sqrt{(1-L)^2+R^2}\right) \tag{27}$$

$$b^s_{eni} \sim \frac{1}{A\pi\gamma_n}\cos(A\pi\gamma)\frac{d}{dt}\left\{J_\nu\left(A\pi\sqrt{t^2+R^2}\right)\cos\left[\nu\left(\tan^{-1}\frac{R}{t}-\alpha\right)\right]\right\}\Big|_{t=1-L} - \frac{1}{A\pi\gamma_n}\frac{d}{dt}\left\{J_\nu\left(A\pi\sqrt{t^2+R^2}\right)\cos\left[\nu\left(\tan^{-1}\frac{R}{t}-\alpha\right)\right]\right\}\Big|_{t=-L} \tag{28}$$

This is valid for larger n, i.e. evanescent orders n.

The indices r and i denote the real and imaginary components. From the relations (24) to (28) it follows that a_{nmr}, a_{nmi}, $a_{nmr}, a_{nmi}, b^{s}_{lni}, b^{s}_{lnr} \sim \frac{1}{n}$ but $b^{p}_{lnr}, b^{p}_{lni} \sim \frac{1}{n^2}$. As it will be seen later, this difference in b^{s}_{ln} and b^{p}_{ln} dependence on n will have a very strong effect on the polarization phenomena. At this point it is important to mention, that b_{ln} is the coupling coefficient that couples the nth freespace order to the lth groove harmonic. In the case of the parallel polarization they decay with n as $\frac{1}{n^2}$ and for the perpendicular polarization as $\frac{1}{n}$. This means that for the perpendicular polarization the nth order is coupled to more groove harmonics and that the interaction between groove harmonics and free space orders is stronger. If these harmonics come into resonance $-k_x d = m\frac{\pi}{2}$ — one would expect stronger effects than in the case of the parallel polarization.

II. Diffraction Anomalies

Developed relations allow us now to discuss various anomalies that can occur on a diffraction grating. One type - the Rayleigh anomalies - are well known. The other type of anomalies - the new anomalies - are mostly much weaker and broader, therefore, more difficult to detect. Expecially strong anomalies will appear if the two types of anomalies coincide. One kind will coincide only with double Rayleigh anomalies.

A. New Anomalies

The relations (12), (13) and (22) for the coefficients a_{nm}, $b^{p}_{\ell n}$ and $b^{s}_{\ell n}$ go through a strong extrema when sine or cosine of $A\pi\gamma$ is equal to zero. The change in value of the matrix coefficients will be reflected in a change of grating spectra. These anomalies will occure at any value of A - or relative wavelength λ/d - but for a set of fixed angles of incidence. There will be two types of these anomalies depending on wheather sine or cosine of $A\pi\gamma$ is zero. The two conditions on the angle of incidence are

$$\varphi_1 = \sin^{-1}\left(\frac{\ell}{2A}\right) \qquad (29)$$

for ℓ even integer and

$$\varphi_2 = \sin^{-1}\left(\frac{\ell}{2A}\right), \qquad (30)$$

where ℓ is an odd integer.

The physical meaning of these conditions is that an anomaly will occur, when the phase change of the incident wave over a groove is either a multiple of π or an odd multiple of $\pi/2$. The Bragg condition $k_x d = \pi$ is just a special case of the first kind of anomaly when $\ell = 2$.

a) φ_1 anomaly: For the anomaly of the first kind, where $A\gamma = \ell/2$ (ℓ even), one can show that

$$\gamma_{-n} = -\gamma_{n-\frac{1}{2}\ell} \tag{32}$$

which than results in

$$\delta_{-n} = \delta_{n-\frac{1}{2}\ell}. \tag{33}$$

This means that the orders are diffracted symmetrically around a special order $n_{sym} = \frac{1}{4}\ell$. If the phase change of the incident wave over the groove is a multiple of 2π then ℓ can be factorized by 4 and n_{sym} is a real order. On the other hand if the phase over the groove is equal to an odd multiple of π, then ℓ can be factorized only by 2 and n_{sym} is a half integer. This means that the direction of symmetry lies between two neighboring orders: $n_{sym} + \frac{\ell}{2}$ and $n_{sym} - \frac{\ell}{2}$. From the relation (32) and (33) it follows that the matrix coefficients a_{nm} and $b^{p,s}_{\ell n}$ are also symmetric about $n_{sym} = \frac{1}{4}\ell$ in complex conjugate sense:

$$a_{-n,m} = a^*_{n-\frac{\ell}{2},m} \tag{34}$$

$$b^{p,s}_{\ell,-n} = \left(b^{p,s}_{\ell,n-\frac{\ell}{2}}\right)^*. \tag{35}$$

This now has a very strong influence on the two sets of linear equations (6) and (7).
Let us denote

$$\sum_{n=-\infty}^{\infty} \delta_n b_{\ell n}^{p,s} a_{nm} - c_{\ell m}^{p,s} = S_{\ell m}^{p,s} - c_{\ell m}^{p,s}$$

so that

$$S_{\ell m}^{p,s} = \sum_{n=-\infty}^{\infty} \delta_n b_{\ell n}^{p,s} a_{nm} . \qquad (36)$$

Because of the complex conjugate symmetry of the matrix coefficients very many terms in the infinite sum cancel out and others again add up so that one obtains for the real and imaginary components of the sum

$$S_{\ell m r}^{p,s} = 2 \sum_{n=\frac{1}{4}\ell + \frac{1}{2}\Delta_{\ell,4k+2}}^{n_g^+ - 1} \delta_{nr} \left(b_{\ell n r}^{p,s} a_{nmr} - b_{\ell n i}^{p,s} a_{nmi} \right) \qquad (37)$$

and

$$S_{\ell m i}^{p,s} = 2 \sum_{n=n_g^+}^{\infty} \delta_{nr} \left(b_{\ell n r}^{p,s} a_{nmr} - b_{\ell n i}^{p,s} a_{nmi} \right). \qquad (38)$$

The indices r and i denote here the real and imaginary components, δ_{nr} is the absolute value of δ_n and n_g^+ is the first positive evanescent order or the grazing order.

$\Delta_{\ell, 4k+2}$ is a Kronecker symbol being equal to 1 for $\ell = 4k + 2$ ($k = 0, \pm 1, \pm 2 \ldots$), otherwise zero.

Under this condition the grating spectrum must experience some change. As it will be seen later, it usually becomes a maximum or minimum and sometimes an inflexion point. It is interesting to point out that only the propagating orders through their coefficients play a role in the real part of the matrix $S^{P,S}_{\ell m}$. On the other hand the imaginary part of $S^{P,S}_{\ell m}$ contains the coupling coefficients of only the evanescent orders.

b) φ_2 anomaly:

The other anomaly φ_2 for $A\pi\gamma = \frac{1}{2}\ell\pi$ (ℓ odd) is less important. One can show that the symmetry lies now at $n_{sym} = \frac{1}{4}\ell$ (ℓ is odd). The symmetry lies a quarter integer away from the first integer order. This then means that the order symmetric to the nth order would be half integer $\gamma_{-n} = \gamma_n - \ell/4$. Being noninteger that order does not exist so the symmetry is destroyed. From relation (12) one obtains for a_{nm}

$$
\begin{aligned}
a_{nm} = \Bigg\{ & (-1)^M \sum_{k=0}^{\infty} \frac{(-1)^k}{(A\pi\gamma_n)^{2k+1}} \frac{d^{2k}}{dt^{2k}} J_\mu \left[A\pi (t^2+R^2)^{\frac{1}{2}}\right]\Big|_{t=1-L} - \\
& - \sum_{k=0}^{\infty} \frac{(-1)^k}{(A\pi\gamma_n)^{2k+2}} \frac{d^{2k+1}}{dt^{2k+1}} J_\mu \left[A\pi (t^2+R^2)^{\frac{1}{2}}\right]\Big|_{t=-L} \Bigg\} + \\
+ i \Bigg\{ & (-1)^M \sum_{k=0}^{\infty} \frac{(-1)^k}{(A\pi\gamma_n)^{2k+2}} \frac{d^{2k+1}}{dt^{2k+1}} J_\mu \left[A\pi (t^2+R^2)^{\frac{1}{2}}\right]\Big|_{t=1-L} + \\
& + \sum_{k=0}^{\infty} \frac{(-1)^k}{(A\pi\gamma_n)^{2k+1}} \frac{d^{2k}}{dt^{2k}} J_\mu \left[A\pi (t^2+R^2)^{\frac{1}{2}}\right]\Big|_{t=-L} \Bigg\},
\end{aligned}
\tag{39}
$$

where $M = \frac{1}{2}(\ell-1)$.

The first term in the real part and the second term in the imaginary part are odd functions of n around n_{sym}. On the other hand the second term of the real part and the first term in the imaginary part are even functions around n_{sym}. Due to this mixing of even and odd functions the change in a_{nm} and $b_{\ell n}^{p,s}$ is not as strong as in the case of φ_1 anomaly. Nevertheless, there will occur some partial cacellations and adding up in $S_{\ell m}^{p,s}$ expressions and that will result in anomalies that will be weaker than φ_1 anomalies.

B. Coincidence of Rayleigh Anomalies with New Anomalies

The Rayleigh anomaly occurs when one of the propagating orders becomes a grazing order, i. e. its direction sine and cosine become $\gamma_n = 1$ and $\delta_n = 0$. An especially interesting case is when two orders, one propagating in positive the other in negative x direction, become evanescent (grazing). The conditions for this double anomaly to occur is that $A = n_g^+ - n_g^-$ and also $A\gamma$ have to be integers.

The Rayleigh anomalies and the new anomalies are shown together, on the γ vs λ/d diagram of the Fig. 2. The lines indicated by n are the Rayleigh conditions, defined by $\gamma = +1 + n\frac{\lambda}{d}$ and $\gamma = -1 + n\frac{\lambda}{d}$. The shaded area between $n = 1$ and $n = -1$ is the region of specular reflection, where the 0 order is the only possible order. Lines indicated by ℓ represent the conditions for the new anomalies: $\gamma = \frac{\ell}{4}\frac{\lambda}{d}$.

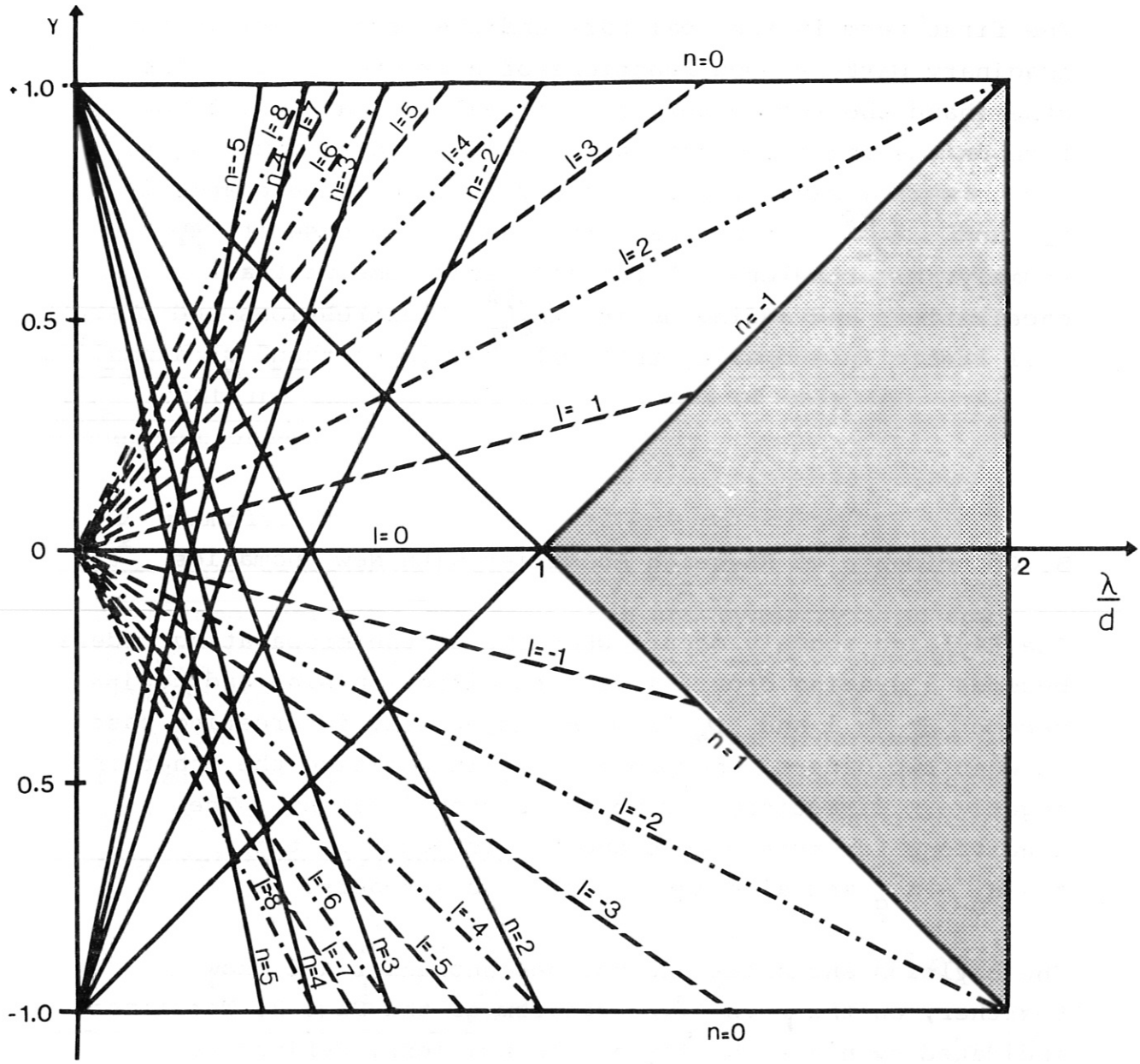

Fig. 2 Calculated anomalies in γ vs. λ/d plane. The n values represent the Rayleigh and l the new anomalies.

At certain values of γ and λ/d the Rayleigh anomaly will coincide with the new anomaly. This is represented by cross points of the two families of lines. Depending whether the Rayleigh line crosses with the line representing the new anomalies of the first kind or the second kind, we will have two types of coincidences.

(a) Coincidence of the Rayleigh anomaly with φ_1 anomaly.

The coincidence anomaly satisfies both conditions for both anomalies. This results in conditions that both A and $A\gamma$ have to be integers. At the same time these are the conditions for the double Rayleigh anomaly. It follows then that the φ_1 anomaly can coincide with a Rayleigh anomaly only as a tripple anomaly. It also follows that every double Rayleigh anomaly is also a new anomaly. However, the opposite is not true: for a constant λ/d and variable φ there are twice as many φ_1 anomalies as double Rayleigh anomalies. Because of this forced coincidence of the double Rayleigh anomaly with the φ_1 anomaly, it can be also concluded that the symmetry relations (32), (33), (34), (35), (37) and (38) are also valid for the double Rayleigh anomaly. The physical meaning of the conditions for the tripple anomaly is, firstly, that the phase diference of the incident wave across the groove is equal to a multiple of π, and secondly, that the dimension of the groove width d is equal to a half multiple of the free space wavelength of the incident wave. It is natural to expect, when these two different resonance conditions are satisfied, that a strong anomaly is to be expected. In the numerical results it will be shown that this is the case. The positions of these strong coincidence anomalies are characterized in Fig. 2 by tripple crossings.

An even stronger anomaly seems to occur with the positive grazing order being +1 order. In this case the $n_{res} = 2-A$ will show very sharp resonant behaviour. This resonant case will be discussed thoroughly in the numerical part. n_{res} is a backscattering order that satisfies simultaneously $n_{res} = A\gamma = -A\gamma_{nres}$ or $\gamma_{nres} = -\gamma$. The last conditions say that the phase jump of both the incident and the backscattered resonance wave is the same and equal to $n_{res}\pi$. Because the diffracted order n_{res} is also in resonance across the groove, one should expect the anomaly to be even more enhanced. These resonances are characterized in diagram of Fig. 2 by a tripple crossing and are situated on the n = 1 line.

b) Coincidence of the Rayleigh anomaly with φ_2 anomaly.

The new anomaly φ_2 can coincide with only single Rayleigh anomalies. Because of the diminished symmetry compared to φ_1 case, these coincidence anomalies are somewhat weaker than those previously described. The conditions for the coincidence are that $A\gamma$ and A be half integers. This will occur firstly, when the phase jump of the incident wave across the groove is equal to and odd multiple of $\pi/2$, and secondly, when the grating constant d is equal to an odd multiple of quarter wavelengths: $d = (2k + 1)\lambda/4$ $(k = 0, 1, 2, 3 \ldots)$.

C. Coincidence of in-blaze wavelength with the new anomaly

In-blaze wavelength is defined, as indicated in Fig 3, by the quasispecular reflection of the order n from the groove facets. The directions of the incident and reflected order

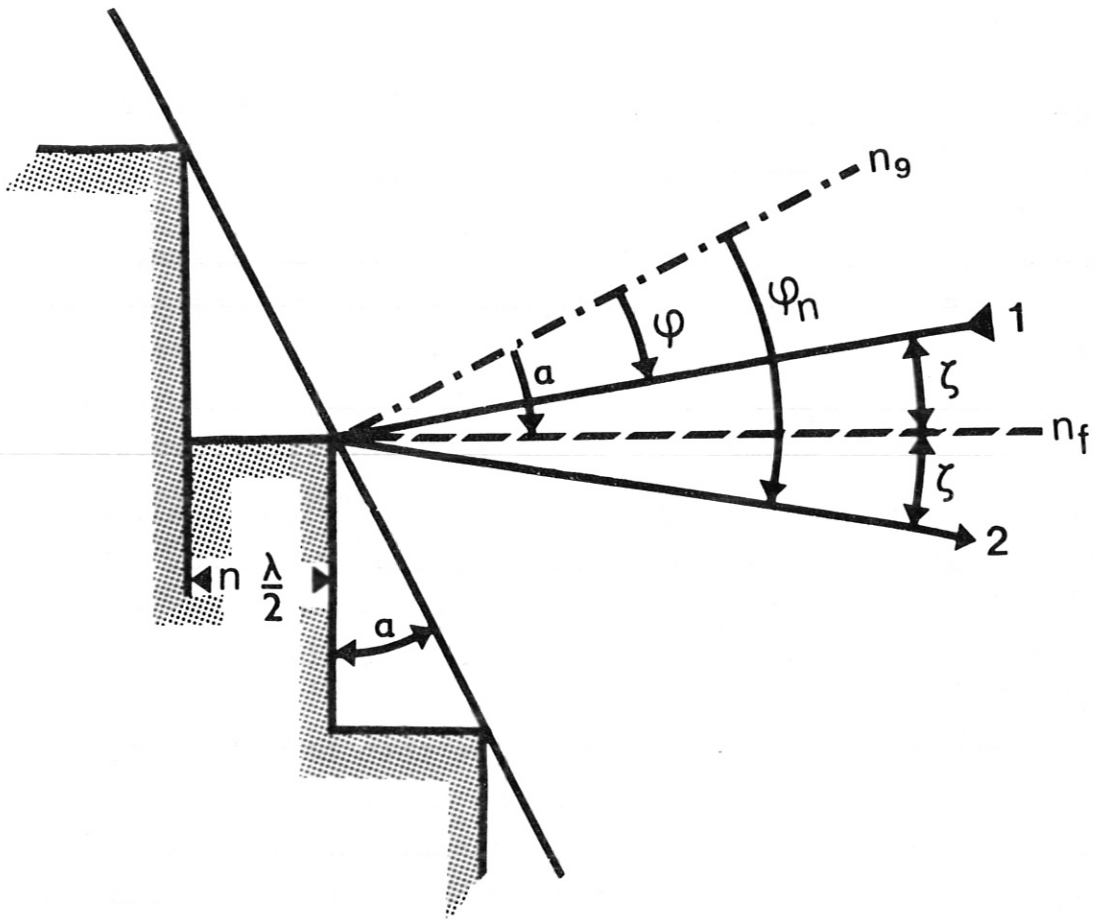

Fig. 3 In-blaze wavelength geometry. n_g is the normal on the grating plane and n_f is the normal on the facet.

are symmetric about the normal on the facet. The angle between two waves is equal to $\theta = 2\zeta$. From the grating equation $\sin\varphi_n = \sin\varphi - n\frac{\lambda}{d}$ and the figure one can see, that the condition for the blazing is given by

$$A \sin\alpha \cos\frac{\theta}{2} = n,$$

where n = ± 1, ± 2 .... is the number of half-wavelengths across the other facet.

If the angle between the incident and reflected wave becomes zero, i.e. $\theta = 0$, then the condition on the blazing obtains the form

$$A\gamma = n,$$

because in this case $\varphi = \alpha$. But this condition is also the condition for the new anomalies of the φ_1 kind. We can, therefore, conclude that the blazing wavelength is only a special case of the new φ_1 anomaly for which $\alpha = \varphi$.

An interesting case is $\alpha = -30°$: we then have A = -2n. For A = 4, we obtain that the blazing order is -2 order. But this is the backscattering resonance, for which we already have a coincidence of two Rayleigh anomalies and φ_1 anomaly. The fact that this is also a blazing order should enhance -2 order resonance even more.

III. Numerical Results

The rigorous solutions for the parallel and perpendicular polarization represented by the two infinite sets of linear equations (6) and (17) and two expressions for the diffracted fields (7) and (18) can be approximated by truncating the matrices at some maximum n, l and m. Typical truncation values utilizied in our numerical analysis where $n_{max} = \pm 16$ and $l_{max} = m_{max} = 10$.

An example of the new anomalies and the single Rayleigh anomalies is given in Fig 4. It shows the power distribution in various orders as a function of the angle of incidence, where $\lambda/d = 0.834$, $\alpha = 10^{o}$ and the polarization is perpendicular. The very sharp and strong Rayleigh are indicated by upper arrows and φ_R . The new anomalies are indicated by the middle arrows for φ_1 and the lower arrows for φ_2 . The φ_1 anomalies are characterized by broad an shallow maxima and minima or inflection points. The φ_2 anomalies are situated very near to Rayleigh anomalies and do not show any characteristic feature.

An example of backscattering resonance - tripple coincidence - again for the perpendicular polarization is shown in Fig 5 for $\lambda/d = 0.5$ (A = 4.0) and $\alpha = 15^{o}$. The resonance occurs for $\varphi = -30^{o}$ and the resonant order is in this case $n_{res} = -2$. The continuous curves are our numerical results and the experimental points of the University of Michigan group[17] are indicated by small circles. The agreement between the theory and experimental points is good. The backscattering resonance is seen experimentally.

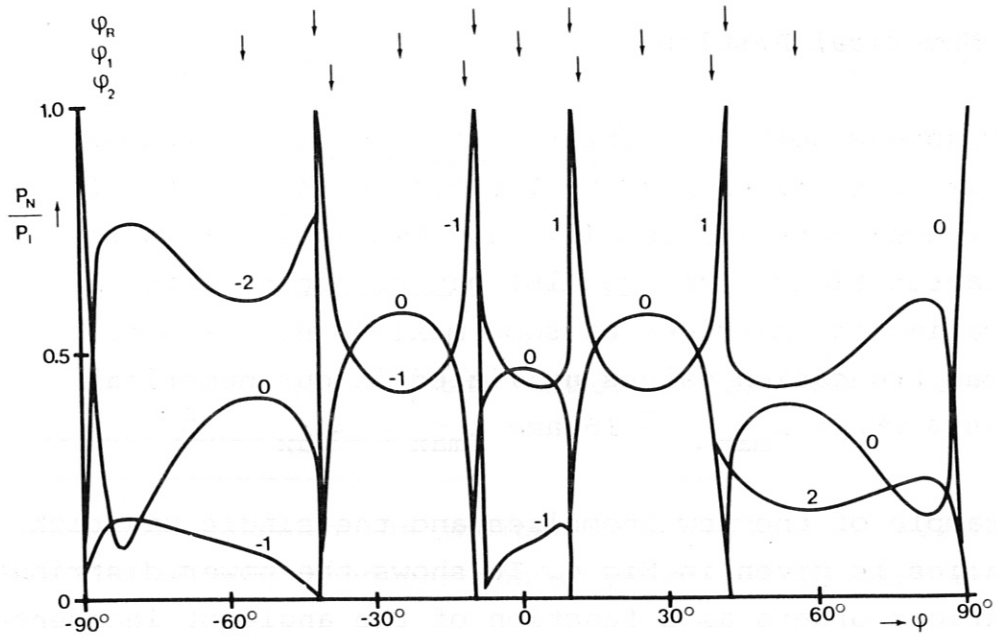

Fig. 4 Irradiance distribution into various orders as a function of angle of incidence φ. The grating parameters are $\alpha = 10^{\circ}$, $\beta = 90^{\circ}$, and $\lambda/d = 0.834$. The upper arrows indicate the Rayleigh and lower the new anomalies.

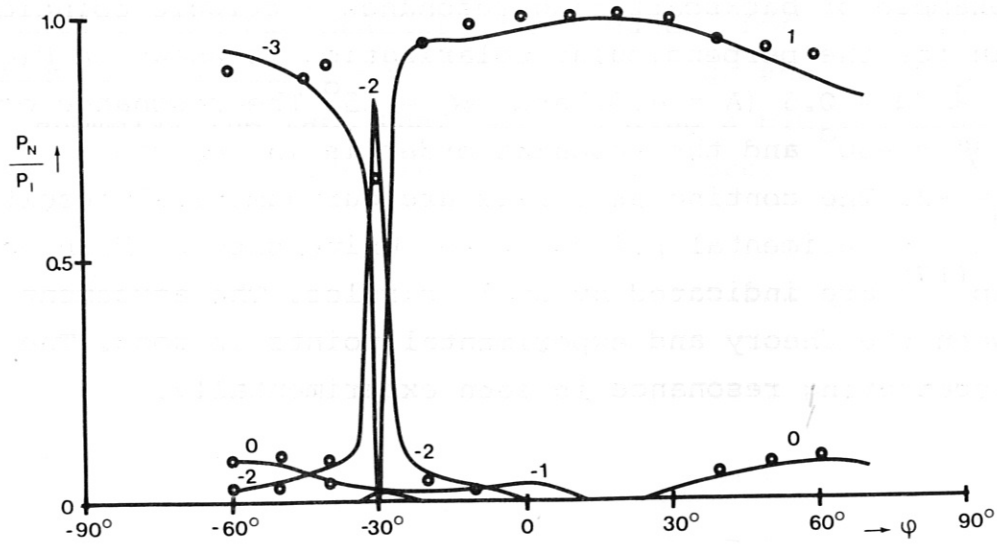

Fig. 5 Irradiance distribution into various orders as a function of angle of incidence φ. The grating parameters are $\alpha = 10^{\circ}$, $\beta = 90^{\circ}$, and $\lambda/d = 0.5$.

This particular resonance is investigated more thoroughly in terms of its dependence on polarization, grating constant α , angle of incidence φ , and the normalized wavelength λ/d or A in the next fourteen figures because of its possible applicability in laser cavities and as spatial and spectral filters. In Figs 6 - 11 the backscattering resonance for A = 4 and $\varphi = -30^{\circ}$ is analyzed. For small α most of the power is in the 0 order. Increasing α, more and more power goes into the grating orders -3 and +1 and into the resonant order -2. The resonance for the perpendicular polarization is very narrow and strong and for the parallel polarization very broad and weak. Parallel resonance becomes more pronounced and sharper with increased α . Note that the interval for the angle of incidence is for the perpendicular polarization 1.6° and for the parallel polarization is 16° so that the difference in sharpness of the resonance for the two polarizations is much larger than the one seen by just comparing the figures. For $\alpha = 15^{\circ}$ and perpendicular polarization more than 95 % of the power goes in the resonance into the resonant backscattering order. Full half-width of this resonance is about 10' (about 3 mrad).

In Figs 12 - 15 the next backscattering resonance for A = 5 and $\alpha = 10^{\circ}$ is investigated. A has been changed by + 0,2 % and -0.5 % to observe the effect on the resonance for the perpendicular polarization. By decreasing A by 0.5 % the power in the resonant -3 order is not reduced substantially but the spatial bandwidth is increased. On the other hand by increasing A by only 0.2 % - decreasing the wavelength - the power into the resonant order went down by more than order of magnitude. For comparison we show resonance effect for the parallel and perpendicular polarization for the resonance value A = 5. Again the φ scale for the parallel resonance is extended by factor 10.

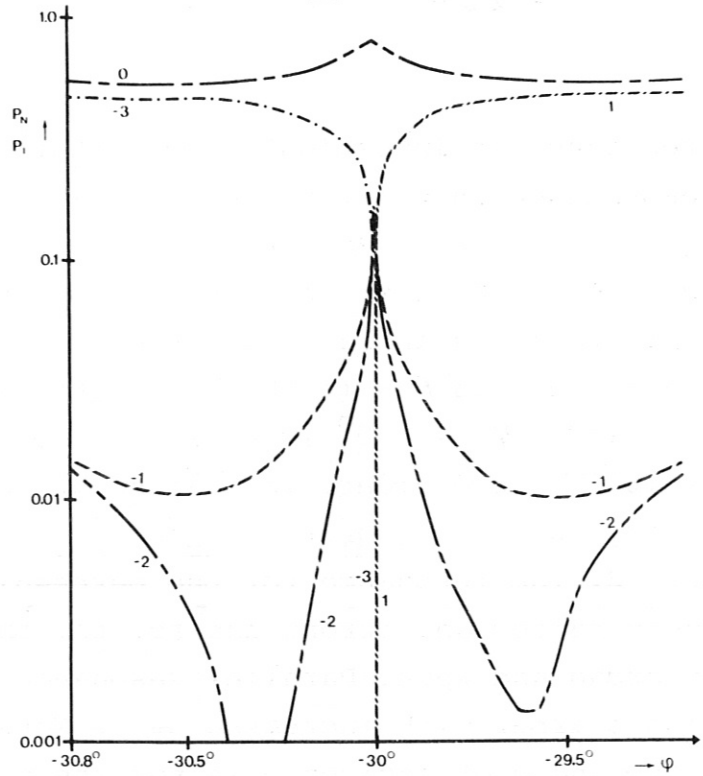

Fig. 6 Irradiance distribution into various orders in the vicinity of the anomaly for $\varphi = -30^{\circ}$ for the perpendicular polarization. The other grating parameters are $\alpha = 5^{\circ}$, $\beta = 90^{\circ}$ and $\lambda/d = 0.5$.

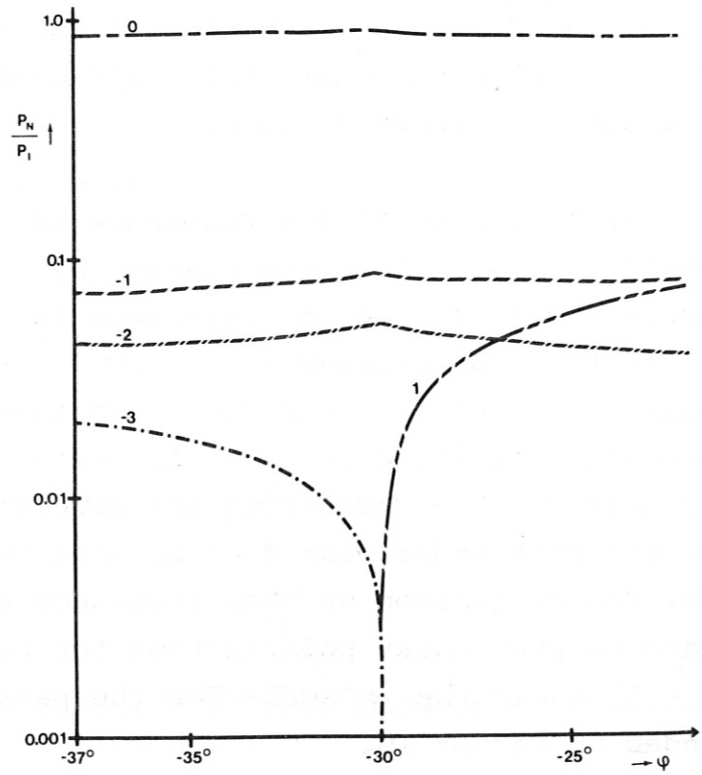

Fig. 7 Irradiance distribution into various orders in the vicinity of the anomaly for $\varphi = -30^{\circ}$ for the parallel polarization. The other grating parameters are as in Fig. 6.

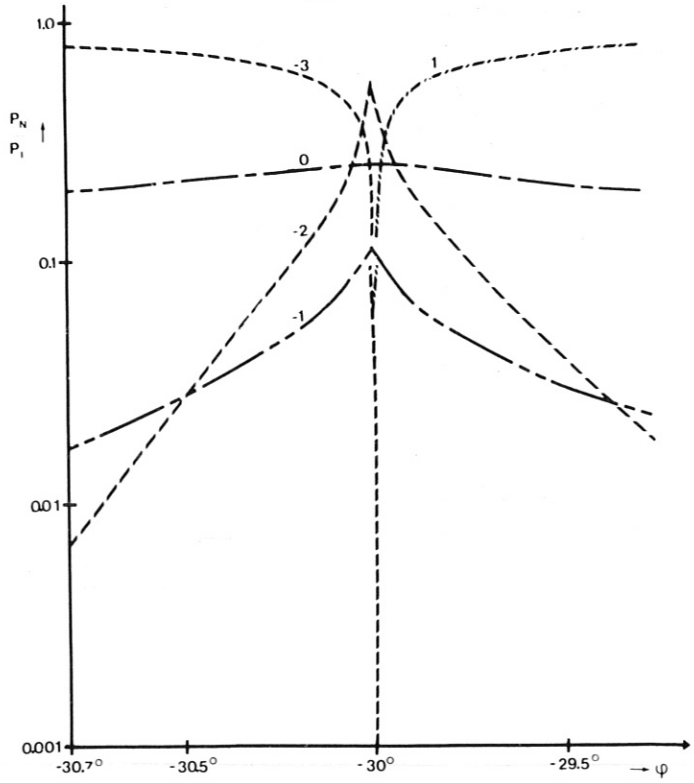

Fig. 8 Irradiance distribution into various orders in the vicinity of the anomaly for $\varphi = -30^{\circ}$ for the perpendicular polarization. The other grating parameters are $\alpha = 10^{\circ}$, $\beta = 90^{\circ}$ and $\lambda/d = 0.5$.

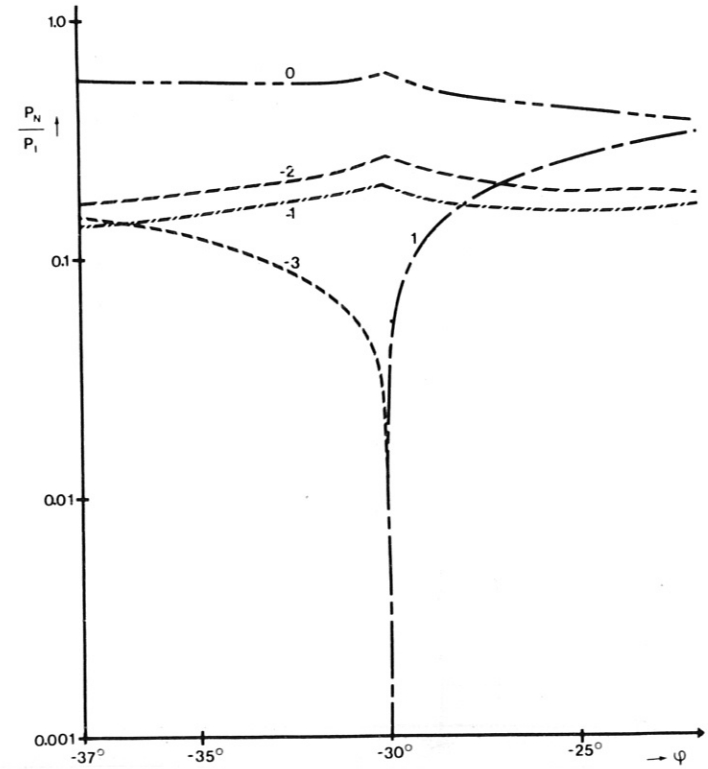

Fig. 9 Irradiance distribution into various orders in the vicinity of the anomaly for $\varphi = -30^{\circ}$ for the parallel polarization. The other grating parameters are as in Fig. 8.

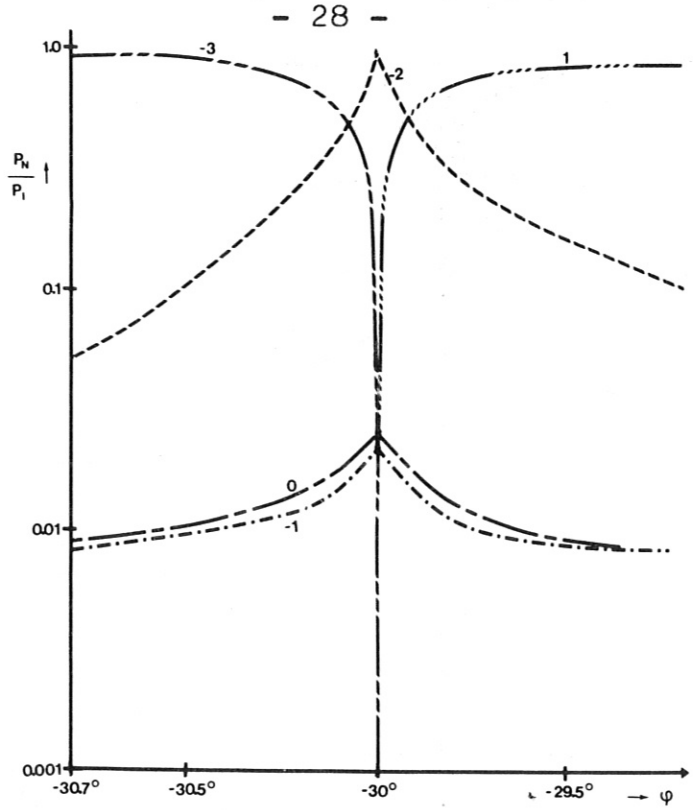

Fig. 10 Irradiance distribution into various orders in the vicinity of the anomaly for $\varphi = -30^{\circ}$ for the parallel polarization. The other grating parameters are $\alpha = 15^{\circ}$, $\beta = 90^{\circ}$ and $\lambda/d = 0.5$.

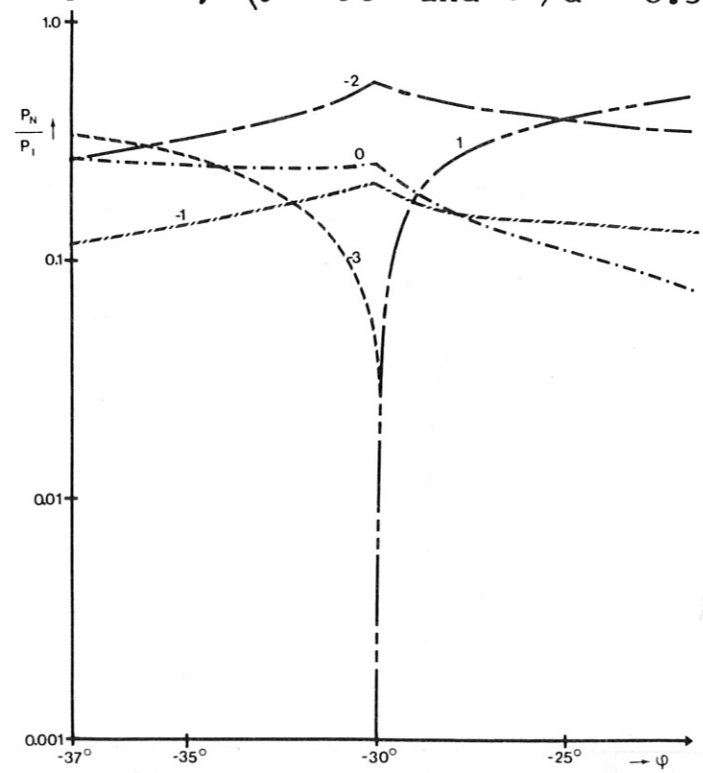

Fig. 11 Irradiance distribution into various orders in the vicinity of the anomaly for $\varphi = -30^{\circ}$ for the parallel polarization. The other grating parameters are as in Fig. 10.

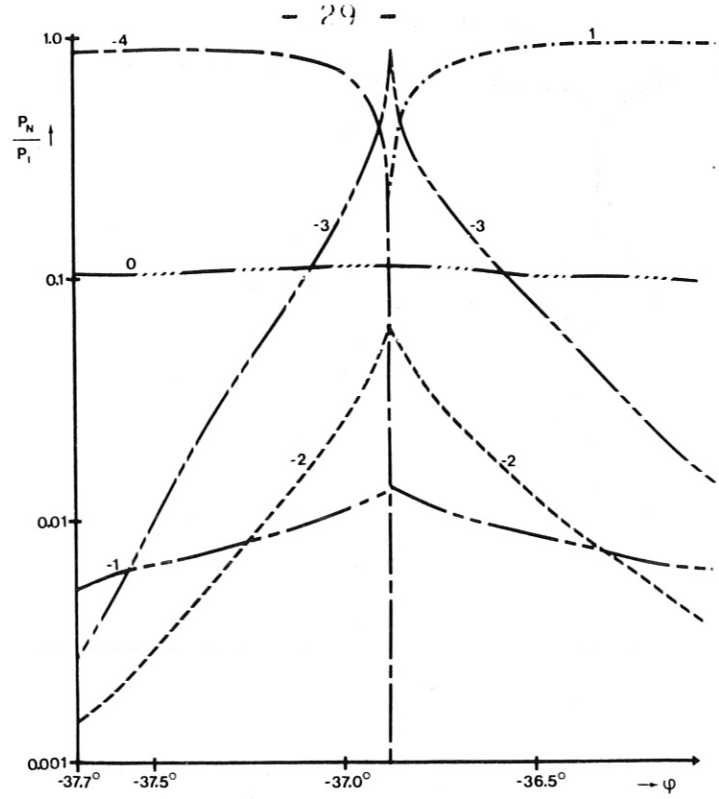

Fig. 12 Irradiance distribution into various orders in the vicinity of the anomaly for $\varphi = -36.87^{\circ}$ for the perpendicular polarization. The other grating parameters are $\alpha = 10^{\circ}$, $\beta = 90^{\circ}$ and $\lambda/d = 0.4$.

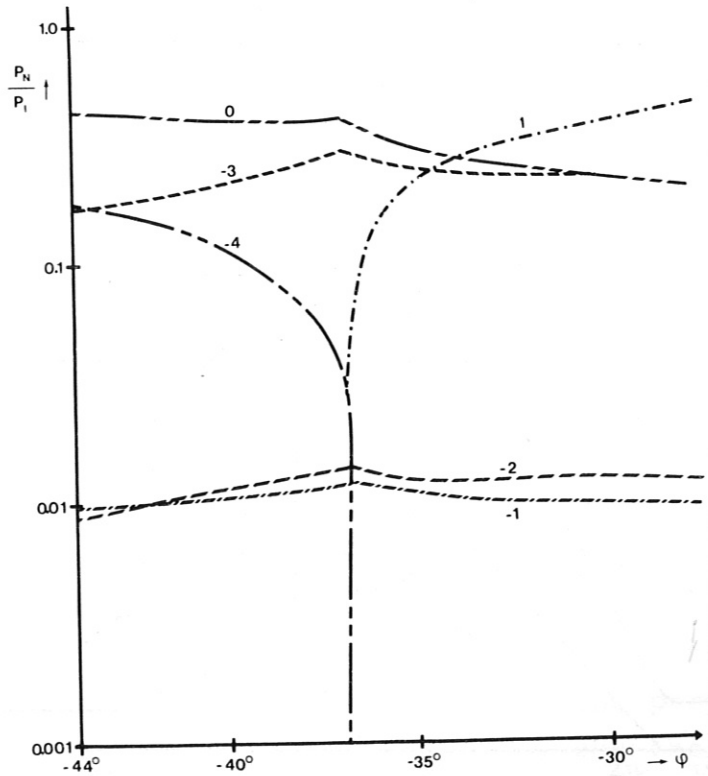

Fig. 13 Irradiance distribution into various orders in the vicinity of the anomaly for $\varphi = -36.87^{\circ}$ for the parallel polarization. The other grating parameters are as in Fig. 12.

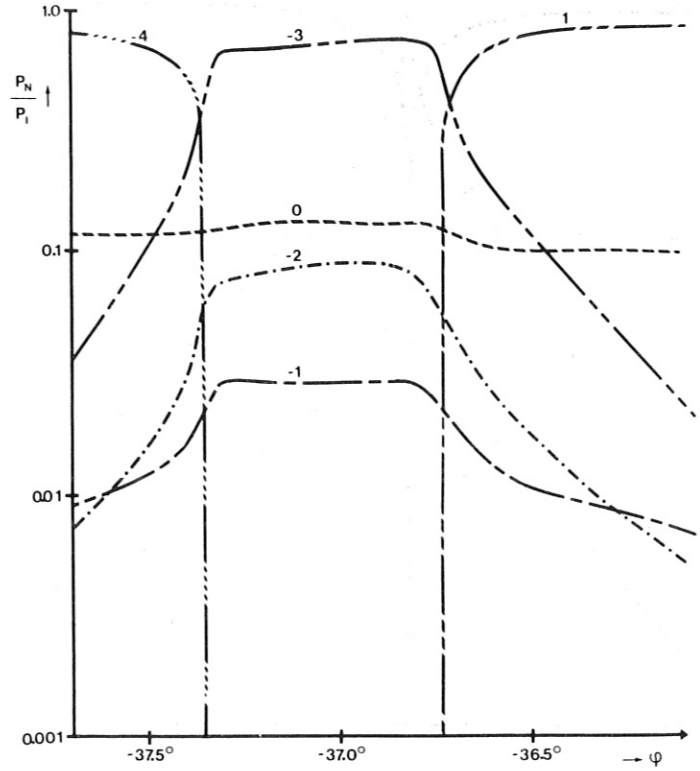

Fig. 14 Irradiance distribution into various orders in the vicinity of the anomaly for $\varphi = -36.87^{\circ}$ for perpendicular polarization. The other grating parameters are $\alpha = 10^{\circ}$, $\beta = 90^{\circ}$ and $\lambda/d = 0.4016$.

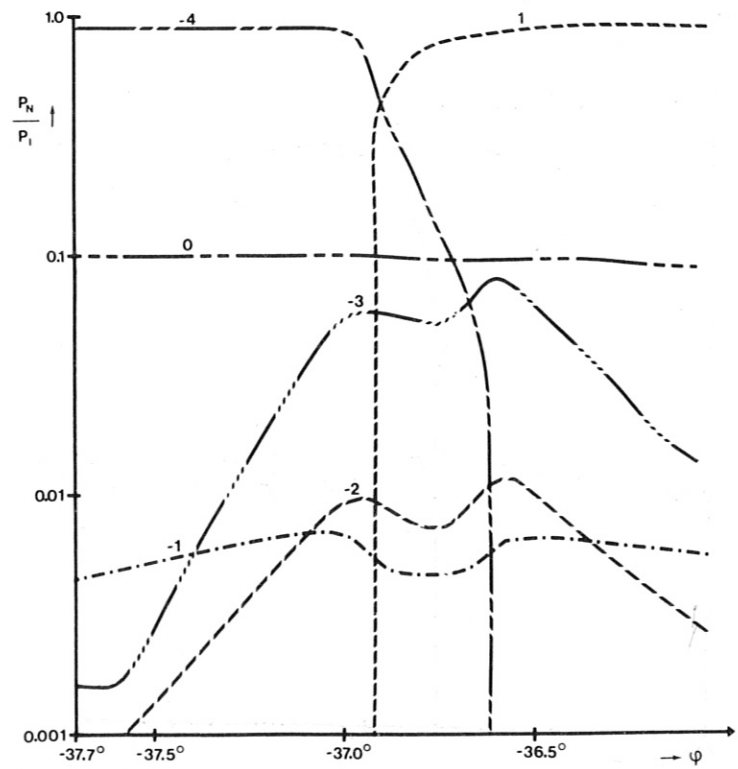

Fig. 15 Irradiance distribution into various orders in the vicinity of the anomaly for $\varphi = -36.87^{\circ}$ for perpendicular polarization. The other grating parameters are $\alpha = 10^{\circ}$, $\beta = 90^{\circ}$ and $\lambda/d = 0.3992$.

Representative studies of the power distribution into various orders for a fixed angle of incidence but with a variable normalized wavelength λ/d and grating constant α are shown in Figs 16 - 18. The polarization is perpendicular. In the first two figures the resonance $\varphi = -30^{\circ}$ and $\lambda/d \sim 0.5$ and for $\alpha = 5^{\circ}$ and 10° is shown. Increasing α to 10° the resonant order -2 rises very fast with λ/d at resonance but then stays at rather high value for longer wavelengths. This can be obviously utilized for the spectral filtering.

The next resonance for $\varphi = -36.867^{\circ}$, $\lambda/d \sim 0.4$ and $\alpha = 5^{\circ}$ and 10° is investigated in Figs 18 and 19. The resonant order -3 shows for $\alpha = 10^{\circ}$ again a sharp filtering characteristic. By increasing α one can obtain even more power into the -3 order and thereby improve the filtering characteristic.

Summary and Conclusions

Integration by parts of matrix coefficients enabled us to obtain these coefficients in terms of infinite sums. From these expressions it is obvious that when the argument becomes equal to a multiple - odd or even - of $\pi/2$ that a new kind of anomaly should be expected. These anomalies are very much amplified, if they are made to coincide with a double Rayleigh anomaly. In an extreme case when one of the grazing orders is + 1 order, then this tripple anomaly becomes a resonance anomaly. In this case the resonance order $n_{res} = 2 - A$ has a very sharp peak for the resonant angle of incidence. This resonance for the perpendicular radiation is extremely sharp; however, for the parallel radiation it is much weaker and broader. The resonance occurs

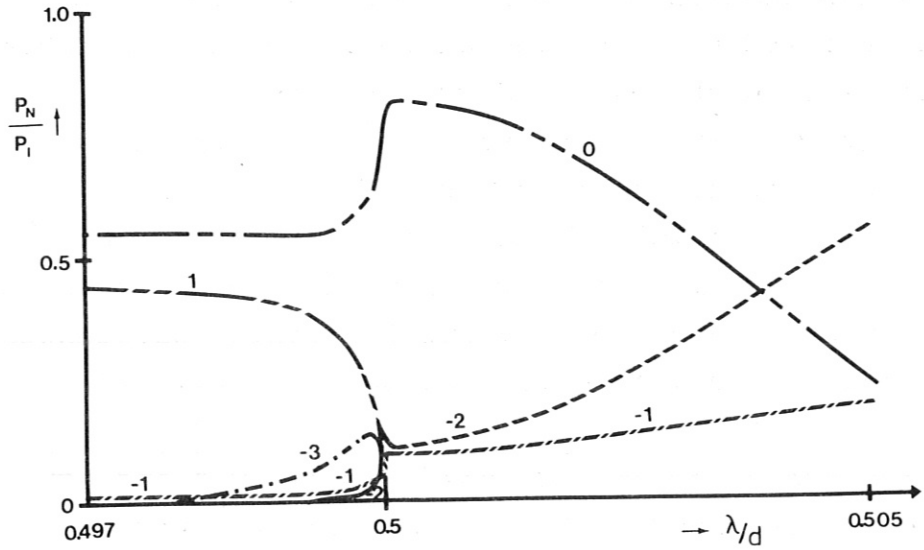

Fig. 16 Irradiance distribution into various orders in the vicinity of the backscattering anomaly for $\lambda/d = 0.5$ for perpendicular polarization. The other grating parameters are $\varphi = -30^{\circ}$, $\alpha = 5^{\circ}$, and $\beta = 90^{\circ}$.

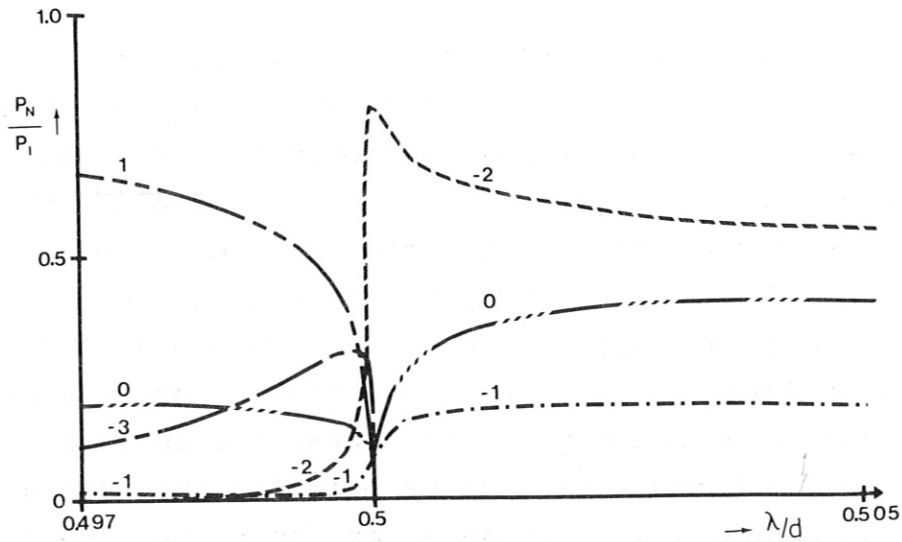

Fig. 17 Irradiance distribution into various orders in the vicinity of the backscattering anomaly for $\lambda/d = 0.5$ for perpendicular polarization. The other grating parameters are $\varphi = -30^{\circ}$, $\alpha = 10^{\circ}$, and $\beta = 90^{\circ}$.

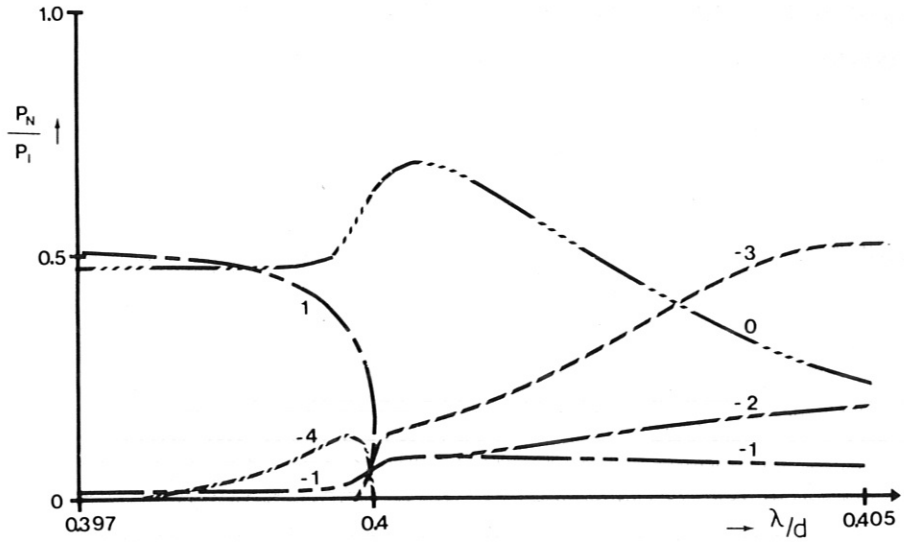

Fig. 18 Irradiance distribution into various orders in the vicinity of the backscattering anomaly for $\lambda/d = 0.4$ for perpendicular polarization. The other grating parameters are $\varphi = -36.87^{\circ}$, $\alpha = 5^{\circ}$, and $\beta = 90^{\circ}$.

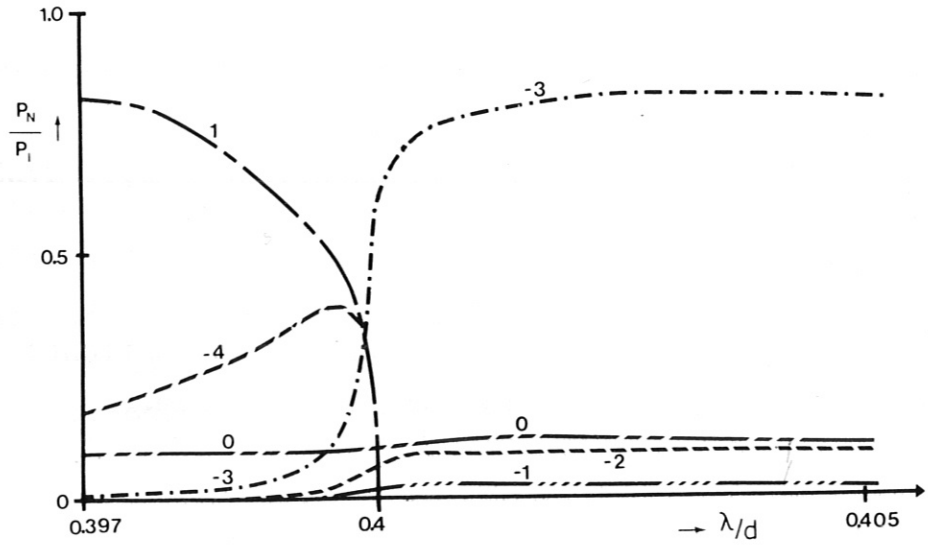

Fig. 19 Irradiance distribution into various orders in the vicinity of the backscattering anomaly for $\lambda/d = 0.4$ for perpendicular polarization. The other grating parameters are $\varphi = -36.87^{\circ}$, $\alpha = 10^{\circ}$, and $\beta = 90^{\circ}$.

for some special fixed λ/d and φ and the power in the resonance order depends on the grating constant α.

This resonance is much sharper than the power distribution maxima around the in-blaze wavelength, that are used sometimes in laser cavities to select a particular lasing line. This effect can be, therefore, used to even stronger reject the other lasing lines and reduce further the number of unwanted longitudinal modes. However, due to the sharpness of the resonance effect, the grating has to be very accurately taylored for a particular lasing line. The machining accuracy of grating should be of the order or better than 1/100. This immediately limits the application of this resonance effect only to submillimeter wave range. The other reason for staying with a longer wavelength is that at very short wavelengths the assumptions, used in the theory, are no more strictly valid. The grating material can not be regarded anymore as a perfect conductor. Due to the losses in the grating surface for the shorter wavelengths these resonances can not be so sharp any more.

Another application of this resonance effect is a band pass filter or a spatial filter. The bandwidth of the band pass filter is directly proportional to the angular divergence and dispersion of the beam coming from the filter grating. A drawback of this application is that the filter is always working very near the backscattering direction. The filtering efficiency (reflectance) is optimized by changing the grating constant α. Here again we can visualize the application only in the far infrared region of the spectrum.

References:

1. R.W. Wood,
Proc.Phys.Soc. (London) 18, 396 (1902).

2. Lord Rayleigh, On the Dynamical Theory of Gratings,
Proc.Phys.Soc. (London) A 79, 399 (1907).

3. C.H. Palmer,Jr., Parallel Diffraction Grating Anomalies,
J.Opt.Soc.Am. 42, 269 (1952).

4. E.A. Yakovlev and F.M. Gerasimov, Experimental Study
of the Intensity Distribution in the Spectrum of
Diffraction Gratings for Polarized Light, Optics
and Spectroscopy 10, 50 (1961).

5. J.E. Stewart and W.S. Gallaway, Diffraction Anomalies
in Grating Spectrophotometers, Appl.Opt. 1, 421 (1962).

6. L.N. Deriugin, The Reflection of a Plane Transvers-
Polarized Wave from a Rectangular Comb,
Radiotekhnika 15, 9 (1960).

7. L.N. Deriugin, Reflection of a Longitudinally Polarized
Wave from a Rectangular Comb,
Radiotekhnika 15, 15 (1960).

8. A. Wirgin and R. Deleuil, Theoretical and Experimental
Investigation of a New Type of Blazed Grating,
J.Opt.Soc.Am. 59, 1348 (1969).

9. R. Deleuil, Réalisation et utilisation d'un appareillage destiné à l'etude des dioptres irréguliers et des réseaux en ondes millimetriques, Opt.Acta 16, 23 (1969).

10. A. Hessel and A.A. Oliner, A New Theory of Wood's Anomalies on Optical Gratings, Appl.Opt. 4, 1275 (1965).

11. C.H. Palmer, F.C. Evering,Jr., and F.M. Nelson, Diffraction Anomalies for Gratings of Rectangular Profile, Appl.Opt. 4, 1271 (1965).

12. V. Twersky, Multiple Scattering of Waves and Optical Phenomena, J.Opt.Soc.Am. 52, 145 (1962).

13. C.H. Palmer and F.W. Phelps,Jr., Grating Anomalies as a Local Phenomenon,J.Opt.Soc.Am. 58, 1184 (1968).

14. F.W. Phelps,Jr. and C.H. Palmer, Radiance of Rectangular Profile Gratings in S Polarization, J.Opt.Soc.Am. 59, 812 (1969).

15. C.H. Palmer and H.W. LeBrun, Anomalous Behavior of Blazed Gratings, Appl.Opt. 11, 907 (1972).

16. S. Jovićević and S. Sesnic, Diffraction of Parallel- and Perpendicular-Polarized Wave from an Echelette Grating, J.Opt.Soc.Am. 62, 865 (1972).

17. C.W. Peters, R.H. Hunt, W.K. Pursley and T.F. Zipf, Microwave Measurements of the Intensity Distribution of Echelette Diffraction Gratings, Report No. 3, (Engineering Research Institute, University of Michigan, Ann Arbor, 1954).